Spin-adapted open-shell time-dependent density functional theory: towards a simple and accurate method for spin-flip-down excitations

Hewang Zhao and Zhendong Li

Key Laboratory of Theoretical and Computational Photochemistry, Ministry of Education, College of Chemistry, Beijing Normal University, Beijing 100875, China

ARTICLE HISTORY

Compiled November 24, 2025

ABSTRACT

A major challenge in using spin-flip time-dependent density functional theory (SF-TD-DFT) for spin-flip-down excitations is the presence of spin contamination. While several improved methods have been developed in the past, a simple and accurate method remains elusive. Here, based on our previous development on spin-adapted open-shell TD-DFT for spin-conserving excitations (X-TD-DFT) [Z. Li and W. Liu, J. Chem. Phys. 135, 194106 (2011)], we introduce a method termed as XSF-TDA for modeling spin-flip-down excitations, and provide an in-depth comparison of different methodologies for mitigating spin contamination in SF-TDA. Pilot applications to prototype systems demonstrate the promise of XSF-TDA over existing SF-TDA methods, including unrestricted SF-TDA (USF-TDA) and mixed-reference SF-TDA (MRSF-TDA), in describing bond breakings and inverted singlet-triplet gap systems.

KEYWORDS

spin-flip; time-dependent density functional theory; spin contamination; spin adaptation $\,$

1. Introduction

Spin-flip time-dependent density functional theory (SF-TD-DFT)[1], which extends the earlier spin-flip framework[2] to TD-DFT, has garnered significant attention for its ability to describe electronic transitions beyond the reach of conventional linear response spin-conserving TD-DFT. For instance, it can be used to study spin-flip transitions in spin-flip emitters[3, 4], which represent a distinct class of luminescent materials that exhibit unique photophysical properties due to spin-forbidden yet radiative transitions. Apart from spin-flip transitions, SF-TD-DFT is also capable of capturing certain double excitations, single-bond dissociation processes, and the correct topology of conical intersections[5, 6, 7], which are notoriously challenging for DFT and spin-conserving TD-DFT within the adiabatic approximation[8].

The initial implementation of SF-TD-DFT by Shao et al.[1] employed a collinear hybrid exchange–correlation (XC) kernel within the Tamm–Dancoff approximation (TDA). This formulation necessitates the use of hybrid XC functionals; pure density functionals would otherwise yield excitation energies that are simply orbital energy differences. Subsequently, Wang and Ziegler introduced a noncollinear XC kernel[9,

Email: zhendongli@bnu.edu.cn

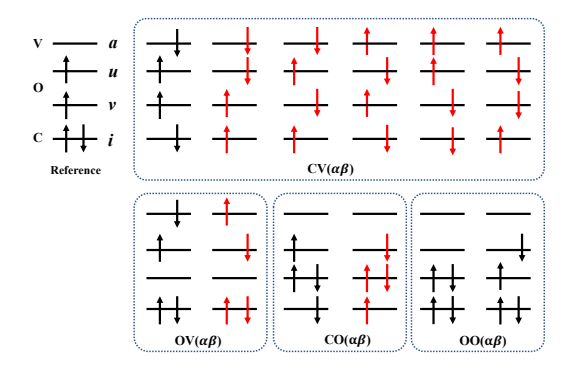


Figure 1. Illustration of the excited-state spin contamination problem in SF-TD-DFT/SF-TDA due to the incompleteness of the excited state manifold generated by spin-flip-down single excitations. Configurations in red color represent the missing higher excitations with respect to the reference to achieve spin completeness/adaptation.

10], which was originally proposed in the context of relativistic TD-DFT for spinor excitations[11, 12, 13], within the local density approximation (LDA) to describe spin-flip excitations in a nonrelativistic framework. Later, full noncollinear XC kernels were implemented for generalized gradient approximation (GGA) and hybrid functionals, both within TDA[14, 15] and in full SF-TD-DFT[16]. However, numerical instabilities can arise with noncollinear GGA kernels. To address this, an adiabatic local density approximation (ALDA0)[16, 17] was introduced, neglecting density gradients in the XC kernel evaluation to enhance numerical stability. More recently, alternative strategies based on a multicollinear formulation have been proposed[18, 19, 20].

A major drawback of SF-TD-DFT is the presence of excited-state spin contamination[21, 22], which arises from the incompleteness of the excitation manifold. We define a subspace as spin complete if it contains all the determinants required to form spin eigenfunctions, and a method as spin-adapted if all its configurations are spin eigenfunctions. Note a subtle distinction: spin-adaptation requires that only spin eigenfunctions are included, but does not necessitate inclusion of all the configurations within a spin-complete subspace. To illustrate the spin contamination issue in SF-TD-DFT, consider a triplet reference system as depicted in Fig. 1. The orbitals of the high-spin open-shell state can be categorized into closed-shell (C), open-shell (O), and virtual-shell (V). We denote a single excitation from an α core orbital to a β virtual orbital as $CV(\alpha\beta)$. It is easy to find that only $OO(\alpha\beta)$ -type spin-flip-down excitations generate a spin-complete subspace. In contrast, the other three types - $CV(\alpha\beta)$, $OV(\alpha\beta)$, and $OV(\alpha\beta)$ - result in spin contamination due to the spin incompleteness of their generated configurations. The determinants shown in red in Fig 1, which are higher excitations than singles with respect to the reference, are necessary to achieve spin completeness/adaptation.

Within wavefunction theory, methods such as spin-complete spin-flip configuration interaction singles (SC-SF-CIS)[23] have been developed to address this issue by directly incorporating the missing higher excitations. However, adapting such approaches to TD-DFT is challenging due to the absence of an explicit wavefunction. Although propagator corrections[21] and generalized excitation operators[24] have been proposed to include higher-order excitations in TD-DFT, these methods have not seen practical application.

Building on the insight that the missing configurations for spin completeness can be accessed from other components of the open-shell reference, one of the present authors developed[22] a spin-adapted random phase approximation (S-RPA) and time-dependent density functional theory (S-TD-DFT) using the tensor equation-of-motion (TEOM) formalism originally introduced in nuclear physics[25]. A key feature of S-RPA is that only single excitations explicitly enter the final matrix elements, while the contributions from higher excitations required for spin-adaptation are implicitly incorporated via the Wigner-Eckart theorem[22]. This crucial property allows for a direct translation of the matrix elements into the TD-DFT framework, leading to S-TD-DFT[26] without the need to go beyond the adiabatic approximation. Subsequently, a more accurate and simpler version, termed X-TD-DFT[27], was introduced to better account for spin degeneracy conditions and to eliminate double counting of correlation for those already spin-adapted states. X-TD-DFT has been shown to achieve accuracy comparable to conventional closed-shell TD-DFT for spin-conserving excitations[28].

For spin-flip-down excitations, a similar strategy can in principle be applied to achieve spin adaptation, as proposed in the original work[22] and later implemented by Zhang and Herbert[5] and Chima and Visscher[29]. However, addressing double counting of correlation in this context is more challenging, as spin contamination affects three types of excitations, and adding the effects of higher excitations for spin-adaptation may deteriorate the excited states dominated by the $OO(\alpha\beta)$ type of excitations, which are already spin-complete. Another relevant approach is the mixed-reference SF-TD-DFT within TDA (MRSF-TDA) proposed by Lee et al.[30, 31], which uses only the $M_S = \pm 1$ components of a triplet reference to mitigate spin contamination, but is not applicable to other spin states. In summary, a general, simple, and accurate spin-adapted method for spin-flip-down excitations is still lacking.

In this work, we present a method termed as XSF-TDA, which extends our previous developments in spin-adapted TD-DFT[22, 26, 27] to spin-flip-down excitations. We introduce a practical approach to alleviate the double counting of correlation resulting from the implicit inclusion of high-order excitations for spin adaptation. Pilot applications on small systems, where high-level theoretical or experimental reference data are available, demonstrate that XSF-TDA performs comparably to unrestricted SF-TDA (USF-TDA) for excited states without significant spin contamination, and consistently outperforms USF-TDA for states exhibiting strong spin contamination. Formal and numerical comparisons are also made between XSF-TDA and MRSF-TDA.

The remainder of this paper is organized as follows. In Sec. 2, we first briefly review the SF-TDA formalism and introduce tensor configuration interaction singles (TCIS) based on the TEOM framework. We then derive XSF-TDA from TCIS and discuss its relationship to existing approaches. Section 3 presents benchmark results obtained with USF-TDA, MRSF-TDA, and XSF-TDA. Conclusions and prospects for future developments are provided in the last section. The following convention for labeling molecular orbitals is used throughout the paper: $\{i, j, k, l, \cdots\}$ for doubly occupied, $\{t, u, v, w, \cdots\}$ for singly occupied, $\{a, b, c, d, \cdots\}$ for unoccupied, and $\{p, q, r, s, \cdots\}$ for unspecified orbitals. Greek indices (e.g., α and β) are used to denote electron spin, and the notation \bar{p} refers to the β spin-orbital corresponding to the α spin-orbital p.

2. Theory

2.1. Spin-flip TD-DFT within the Tamm-Dancoff approximation (SF-TDA)

The SF-TDA for spin-flip-down excitations amounts to solving the following eigenvalue problem

$$\mathbf{A}^{\text{SF-TDA}}\mathbf{X}_{\lambda} = \omega_{\lambda}\mathbf{X}_{\lambda},\tag{1}$$

where the matrix elements of $\mathbf{A}^{\text{SF-TDA}}$ are given by

$$A_{\bar{p}q,\bar{r}s}^{\text{SF-TDA}} = \delta_{qs} f_{pr}^{\beta} - \delta_{pr} f_{sq}^{\alpha} + K_{\bar{p}q,\bar{r}s}. \tag{2}$$

The Kohn-Sham matrix f^{σ} for spin σ is generally expressed as

$$f_{pq}^{\sigma} = h_{pq}^{\sigma} + \sum_{i\sigma'} (p_{\sigma}q_{\sigma}|i_{\sigma'}i_{\sigma'}) + (p_{\sigma}|v_{XC}^{\sigma}|q_{\sigma}) - \sum_{i\sigma'} c_{X}(p_{\sigma}i_{\sigma'}|i_{\sigma'}q_{\sigma}),$$

$$(3)$$

which is applicable to LDA, GGA, and hybrid functionals. Here, h^{σ} denotes the oneelectron term including kinetic energy and nuclear attraction; the second term represents the Coulomb repulsion in Mulliken notation; v_{XC}^{σ} is the exchange–correlation (XC) potential for spin σ ; and the last term introduces exact exchange, with c_{X} denoting the fraction of exact exchange in hybrid functionals. The coupling matrix elements $K_{\bar{p}q,\bar{r}s}$ take the general form

$$K_{\bar{p}q,\bar{r}s} = -c_{\mathcal{X}}(\bar{p}\bar{r}|sq) + [K_{\mathcal{X}\mathcal{C}}]_{\bar{p}q,\bar{r}s},\tag{4}$$

where the exchange–correlation kernel $[K_{XC}]_{\bar{p}q,\bar{r}s}$ for spin-flip excitations depends on the parameterization of the XC functional. While this term vanishes for collinear functionals, it is expressed for noncollinear functionals as[9]

$$[K_{\rm XC}]_{\bar{p}q,\bar{r}s} = \int \psi_{\bar{p}}(\mathbf{r})\psi_{q}(\mathbf{r}) \left[\frac{v_{\rm XC}^{\alpha}(\mathbf{r}) - v_{\rm XC}^{\beta}(\mathbf{r})}{\rho_{\alpha}(\mathbf{r}) - \rho_{\beta}(\mathbf{r})} \right] \psi_{s}(\mathbf{r})\psi_{\bar{r}}(\mathbf{r})d\mathbf{r}.$$
 (5)

Although noncollinear functionals are theoretically more general than their collinear counterparts, the evaluation of Eq. (5) for GGA-type functionals can encounter numerical instabilities in regions where $\rho_{\alpha}(\mathbf{r}) \approx \rho_{\beta}(\mathbf{r})$ but $\nabla \rho_{\alpha}(\mathbf{r}) \neq \nabla \rho_{\beta}(\mathbf{r})$. To mitigate this issue, the ALDA0 kernel[16] is introduced, which effectively neglects density gradient contributions in Eq. (5) by setting $\nabla \rho_{\sigma} = 0$ in computing v_{XC}^{σ} . In this work, we adopt the ALDA0 kernel for GGA and hybrid functionals. The application of multicollinear functionals[18, 19] will be explored in future studies.

2.2. Tensor configuration interaction singles (TCIS)

We mainly focus on TDA in this work, and will use a CIS analog of TEOM, referred to as tensor configuration interaction singles (TCIS). Another important motivation for this choice is that TEOM will lead to non-Hermitian equations for spin-flip-down excitations. To illustrate their differences, we first reexamine the conventional CIS and EOM. Consider the following CI-like equation for an excitation operator $\hat{O}_{\lambda}^{\dagger}$ for the

 λ -th excited state,

$$(\hat{H} - E_0)\hat{O}_{\lambda}^{\dagger}|0\rangle = \omega_{\lambda}\hat{O}_{\lambda}^{\dagger}|0\rangle, \tag{6}$$

where $|0\rangle$ denotes the reference, $E_0 = \langle 0|\hat{H}|0\rangle$ is the reference energy, and ω_{λ} represents the excitation energy. When $\hat{O}_{\lambda}^{\dagger} = \sum_{J} q_{J}^{\dagger} X_{J,\lambda}$ is expanded in an operator basis $\{q_{J}^{\dagger}\}$, the expansion coefficients $X_{J,\lambda}$ can be determined by solving an Hermitian eigenvalue problem

$$\sum_{J} \langle 0|q_{I}(\hat{H} - E_{0})q_{J}^{\dagger}|0\rangle X_{J,\lambda} = \omega_{\lambda} \sum_{J} \langle 0|q_{I}q_{J}^{\dagger}|0\rangle X_{J,\lambda}, \tag{7}$$

It differs from the EOM formulation (of the first kind[22])

$$\sum_{J} \langle 0|q_{I}[\hat{H}, q_{J}^{\dagger}]|0\rangle X_{J,\lambda} = \omega_{\lambda} \sum_{J} \langle 0|[q_{I}, q_{J}^{\dagger}]|0\rangle X_{J,\lambda}, \tag{8}$$

in two aspects. First, if the de-excitation operator q_I satisfies the 'killer condition' $q_I|0\rangle = 0$, then the right-hand sides (RHS) of Eqs. (7) and (8) become identical. Second, the left-hand sides (LHS) of Eqs. (7) and (8) coincide if the condition $\langle 0|q_Iq_J^{\dagger}|0\rangle E_0 = \langle 0|q_Iq_J^{\dagger}\hat{H}|0\rangle$ holds. While these two conditions are satisfied in standard CIS and EOM treatments of closed-shell systems, they may not hold in the case of TCIS and TEOM for spin-flip-down excitations in open-shell systems, as will be discussed later in Sec. 2.4.

To obtain TCIS for spin-adaptation of spin-flip-down excitations, the single excitation operators are recombined to form a triplet excitation operator $T_{pq}^{\dagger}(1)$ defined as follows[32]

$$T_{pq}^{\dagger}(1,1) = -p_{\alpha}^{\dagger}q_{\beta}, \tag{9}$$

$$T_{pq}^{\dagger}(1,0) = \frac{1}{\sqrt{2}}(p_{\alpha}^{\dagger}q_{\alpha} - p_{\beta}^{\dagger}q_{\beta}), \tag{10}$$

$$T_{pq}^{\dagger}(1,-1) = p_{\beta}^{\dagger}q_{\alpha}, \tag{11}$$

where $p_{\alpha}^{(\dagger)}$ denotes the annihilation (creation) operator. A tensor reference $|S_i\rangle\rangle$ is defined as the collection of all components of a spin multiplet $\{|S_iM_i\rangle:M_i=-S_i,\ldots,S_i\}$ with initial spin S_i . The excited configuration $|S_f\rangle\rangle_{pq}$ resulting from the actions of $T_{pq}^{\dagger}(1)$ on $|S_i\rangle\rangle$ is expressed as

$$|S_f\rangle\rangle_{pq} = [T_{pq}^{\dagger}(1) \times |S_i\rangle\rangle]^{S_f},$$
 (12)

where $S_f = S_i - 1$ is considered in this work. For spin-flip-down single excitations, the excited configurations can be generated by CV(1), CO(1), OV(1), and OO(1) type of excitations, where the symbol CV(1) denotes operators of form $T_{ai}^{\dagger}(1)$. For the OO(1) type of excitations, it is useful to distinguish cases where $t \neq u$ from those where t = u in $T_{tu}^{\dagger}(1)$. We adopt the notation $O_1O_2(1)$ for $t \neq u$ and $O_1O_1(1)$ for t = u, respectively. The complete operator basis for excited states with spin $S_f = S_i - 1$ is

thus given by

$$\{q_J^{\dagger}\} = \{T_{\text{CV}}^{\dagger}(1), T_{\text{CO}}^{\dagger}(1), T_{\text{OV}}^{\dagger}(1), T_{\text{O_1O_2}}^{\dagger}(1), T_{\text{O_1O_1}}^{\dagger}(1)\}. \tag{13}$$

The spin-adapted counterpart of Eq. (7), referred to as TCIS, can be obtained in the same way as TEOM[22]

$$\mathbf{M}_{S_f} \mathbf{X}_{\lambda} = \omega_{\lambda} \mathbf{N}_{S_f} \mathbf{X}_{\lambda}, \tag{14}$$

where both \mathbf{M}_{S_f} and \mathbf{N}_{S_f} are Hermitian. The overlap matrix \mathbf{N}_{S_f} corresponding to the operator basis defined in Eq. (13) is block-diagonal

$$\mathbf{N}_{S_{f}} = \mathbf{N}_{S_{f}}^{\text{CV}} \oplus \mathbf{N}_{S_{f}}^{\text{CO}} \oplus \mathbf{N}_{S_{f}}^{\text{OV}} \oplus \mathbf{N}_{S_{f}}^{\text{O}_{1}\text{O}_{2}} \oplus \mathbf{N}_{S_{f}}^{\text{O}_{1}\text{O}_{1}},
[\mathbf{N}_{S_{f}}^{\text{CV}}]_{ai,bj} = \delta_{ij}\delta_{ab},
[\mathbf{N}_{S_{f}}^{\text{CO}}]_{ui,vj} = \frac{2S_{i}+1}{2S_{i}}\delta_{ij}\delta_{uv},
[\mathbf{N}_{S_{f}}^{\text{OV}}]_{au,bv} = \frac{2S_{i}+1}{2S_{i}}\delta_{uv}\delta_{ab},
[\mathbf{N}_{S_{f}}^{\text{O}_{1}\text{O}_{2}}]_{tu,vw} = \frac{2S_{i}+1}{2S_{i}-1}\delta_{tv}\delta_{uw}, \quad t \neq u, v \neq w,
[\mathbf{N}_{S_{f}}^{\text{O}_{1}\text{O}_{1}}]_{tt,vv} = \frac{2S_{i}+1}{2S_{i}-1}(\delta_{tv}-\frac{1}{2S_{i}}).$$
(15)

These expressions indicate that the configurations defined by Eqs. (12) and (13) are generally non-orthonormal. We can first apply the following scaling transformation

$$\mathbf{W} = \mathbf{I}^{\text{CV}} \oplus \sqrt{\frac{2S_i}{2S_i + 1}} \mathbf{I}^{\text{CO}} \oplus \sqrt{\frac{2S_i}{2S_i + 1}} \mathbf{I}^{\text{OV}} \oplus \sqrt{\frac{2S_i - 1}{2S_i + 1}} \mathbf{I}^{\text{O}_1 \text{O}_2} \oplus \sqrt{\frac{2S_i - 1}{2S_i + 1}} \mathbf{I}^{\text{O}_1 \text{O}_1},$$
(16)

such that all configurations become orthonormal except for the O_1O_1 type. The metric for this type of excitations is of rank $N_O - 1$, where $N_O = 2S_i$ denotes the number of open-shell orbitals, because their equal superposition simply yields another component of the reference, viz.,

$$\sum_{i} T_{tt}^{\dagger}(1,-1)|S_{i}S_{i}\rangle = \hat{S}_{-}|S_{i}S_{i}\rangle \propto |S_{i}(S_{i}-1)\rangle. \tag{17}$$

An orthonormal set of spin-adapted basis for $S_f = S_i - 1$ can be generated by an isometry $\mathbf{V} = \mathbf{I}^{\text{CV}} \oplus \mathbf{I}^{\text{CO}} \oplus \mathbf{I}^{\text{OV}} \oplus \mathbf{I}^{\text{O}_1\text{O}_2} \oplus \mathbf{V}^{\text{O}_1\text{O}_1}$, whose nontrivial block $\mathbf{V}^{\text{O}_1\text{O}_1}$ is an

 $N_{\rm O} \times (N_{\rm O} - 1)$ matrix that can be chosen as [33]

$$\mathbf{V}^{O_{1}O_{1}} = \begin{bmatrix} \frac{N_{O}-1}{\sqrt{N_{O}(N_{O}-1)}} & 0 & \dots & 0\\ -\frac{1}{\sqrt{N_{O}(N_{O}-1)}} & \frac{N_{O}-2}{\sqrt{(N_{O}-1)(N_{O}-2)}} & \dots & 0\\ \vdots & \vdots & \ddots & \vdots\\ -\frac{1}{\sqrt{N_{O}(N_{O}-1)}} & -\frac{1}{\sqrt{(N_{O}-1)(N_{O}-2)}} & \dots & \frac{1}{\sqrt{2}}\\ -\frac{1}{\sqrt{N_{O}(N_{O}-1)}} & -\frac{1}{\sqrt{(N_{O}-1)(N_{O}-2)}} & \dots & -\frac{1}{\sqrt{2}} \end{bmatrix},$$
(18)

where the equal superposition is eliminated. A summary of the final orthonormalized excited configurations is provided in Table 1.

Table 1. Orthonormalized excited configurations for $S_f = S_i - 1$. The matrix elements $V_{t,k}$ ($k = 1, \dots, N_{\rm O} - 1$) are given in Eq. (18). $N_{\rm C}$, $N_{\rm O}$, and $N_{\rm V}$ refer to the number of close-shell, open-shell, vacant-shell orbitals, respectively.

type	dim	excited configuration	expanded form for the high-spin component
CV(1)	$N_{ m C}N_{ m V}$	$[T_{ai}^{\dagger} imes S_i angle angle]^{S_f}$	$\sqrt{rac{2S_i-1}{2S_i+1}}\left(\Psi_i^{ar{a}} angle-rac{1}{2S_i}\sum_t(\Psi_{it}^{aar{t}} angle- \Psi_{ar{i}t}^{ar{a}ar{t}} angle) ight)$
			$-rac{1}{2S_i\sqrt{(2S_i+1)(2S_i-1)}}\sum_{tu}\ket{\Psi_{ar{i}ut}^{aar{u}ar{t}}}$
CO(1)	$N_{\rm C}N_{\rm O}$	$\sqrt{\frac{2S_i}{2S_i+1}} [T_{ui}^{\dagger} \times S_i\rangle\rangle]^{S_f}$	$ \Psi_i^{ar{u}} angle\sqrt{rac{2S_i-1}{2S_i}} + \sum_t \Psi_{ar{i}t}^{ar{u}ar{t}} anglerac{1}{\sqrt{2S_i(2S_i-1)}}$
OV(1)	$N_{ m O}N_{ m V}$	$\sqrt{\frac{2S_i}{2S_i+1}} [T_{au}^{\dagger} \times S_i\rangle\rangle]^{S_f}$	$ \Psi_u^{ar{a}} angle\sqrt{rac{2S_i-1}{2S_i}}-\sum_t \Psi_{ut}^{aar{t}} anglerac{1}{\sqrt{2S_i(2S_i-1)}}$
$O_1O_2(1)$	$N_{\rm O}(N_{\rm O}-1)$	$\sqrt{\frac{2S_i-1}{2S_i+1}} [T_{tu}^{\dagger} \times S_i\rangle\rangle]^{S_f}$	$ \Psi_u^{ar{t}} angle\;(t eq u)$
$O_1O_1(1)$	$N_{\rm O}-1$	$\sqrt{\frac{2S_i-1}{2S_i+1}} \sum_t [T_{tt}^{\dagger} \times S_i\rangle]^{S_f} V_{t,k}$	$\sum_{t} (\Psi_{t}^{\bar{t}}\rangle - \frac{1}{2S_{i}} \sum_{v} \Psi_{v}^{\bar{v}}\rangle) V_{t,k} = \sum_{t} \Psi_{t}^{\bar{t}}\rangle V_{t,k}$

Using Eqs. (16) and (18), we can transform Eq. (14) into a standard eigenvalue problem

$$\tilde{\mathbf{A}}^{\text{TCIS}}\tilde{\mathbf{X}}_{\lambda} = \omega_{\lambda}\tilde{\mathbf{X}}_{\lambda},\tag{19}$$

where $\tilde{\mathbf{A}}^{\text{TCIS}}$ is defined by

$$\tilde{\mathbf{A}}^{\text{TCIS}} = \mathbf{V}^T \mathbf{A}(S_i) \mathbf{V}, \quad \mathbf{A}(S_i) = \mathbf{W}^T \mathbf{M} \mathbf{W}.$$
 (20)

Here, the subscript S_f has been omitted for brevity, but the dependence on S_i in $\mathbf{A}(S_i)$ is explicitly indicated. Following the approach detailed in Ref. [22], we can find all matrix elements of $\mathbf{A}(S_i)$, which are summarized in Table 2. It is important to note that the resulting matrix $\mathbf{A}(S_i)$ is not equivalent to that of SC-SF-CIS[23], as its dimension is exactly the same as that of SF-CIS, while SC-SF-CIS contains more configurations for spin-completeness. For instance, considering the $\mathrm{CV}(\alpha\beta)$ type of excitations illustrated in Fig. 1, TCIS only contains one spin-adapted configuration generated from Eq. (12), whereas SC-SF-CIS includes all the two spin-adapted singlet configurations from the the six underlying determinants. A key advantage of TCIS lies in that its ability to seamlessly bridge the spin-contaminated SF-CIS with a spin-adapted formulation. Specifically, taking the limit $S_i \to \infty$ in $\mathbf{A}(S_i)$ recovers the conventional SF-CIS matrix elements $\mathbf{A}(\infty)$. This property enables a natural extension of our previously developed X-TD-DFT framework for spin-conserving excitations[27], facilitating the construction of the XSF-TDA method for spin-flip-down excitations.

Table 2. Matrix elements of $\mathbf{A}(S_i)$ in Eq. (20) for TCIS. Only the upper triangular parts are presented as the matrix is Hermitian. In the limit of $S_i \to \infty$, all the matrix elements go to those in SF-CIS, i.e., Eq. (2) with $c_{\rm X}=1$. The matrix elements f_{pq}^S is defined by $f_{pq}^S=\frac{1}{2}(f_{pq}^\beta-f_{pq}^\alpha)=\frac{1}{2}\sum_t(pt|tq)$.

	$v p q \qquad v p q \qquad 2 (v p q \qquad v p q) \qquad 2 \simeq l (v + 1)$
block	matrix elements
CV(1)- $CV(1)$	$A_{ai,bj} = \delta_{ij} f_{ab}^{\beta} - \delta_{ab} f_{ji}^{\alpha} + \frac{1}{S_i} \delta_{ij} f_{ab}^{S} + \frac{1}{S_i} \delta_{ab} f_{ji}^{S} - (ab ji)$
CO(1)- $CO(1)$	$A_{ui,vj} = \delta_{ij} f_{uv}^{\beta} - \delta_{uv} f_{ji}^{\alpha} + \frac{2}{2S_{i-1}} \delta_{uv} f_{ji}^{S} - (uv ji) - \frac{1}{2S_{i-1}} (ui jv)$
OV(1)- $OV(1)$	$A_{au,bv} = \delta_{uv} f_{ab}^{\beta} - \delta_{ab} f_{uv}^{\alpha} + \frac{2}{2S_i - 1} \delta_{uv} f_{ab}^{S} - (ab vu) - \frac{1}{2S_i - 1} (au vb)$
CV(1)- $CO(1)$	$A_{ai,vj} = \sqrt{\frac{2S_i + 1}{2S_i}} \delta_{ij} f_{av}^{\beta} - \sqrt{\frac{2S_i + 1}{2S_i}} (av ji)$
CV(1)- $OV(1)$	$A_{ai,bv} = -\sqrt{rac{2S_i+1}{2S_i}}\delta_{ab}f_{vi}^{lpha} - \sqrt{rac{2S_i+1}{2S_i}}(ab vi)$
CO(1)- $OV(1)$	$A_{ui,bv} = -\frac{{}^{\backprime}_{2S_i}}{{}^{\backprime}_{2S_i-1}}(ub vi) + \frac{{}^{\backprime}_{1}}{{}^{\backprime}_{2S_i-1}}(ui vb)$
OO(1)- $OO(1)$	$A_{tu,vw} = \delta_{wu} f_{tv}^{\beta} - \delta_{tv} f_{uw}^{\alpha} - (tv wu)$
CV(1)- $OO(1)$	$A_{ai,vw} = \sqrt{\frac{2S_i + 1}{2S_i - 1}} (\delta_{vw} \frac{1}{S_i} f_{ia}^s - (av wi))$
CO(1)- $OO(1)$	$A_{ui,vw} = \sqrt{\frac{2S_i}{2S_i - 1}} (-\delta_{vu} f_{iw}^{\alpha} - (uv wi)) + \frac{1}{\sqrt{2S_i(2S_i - 1)}} \delta_{vw} f_{iu}^{\beta}$
OV(1)-OO(1)	$A_{au,vw} = \sqrt{\frac{2S_i}{2S_i - 1}} (\delta_{wu} f_{av}^{\beta} - (av wu)) - \frac{1}{\sqrt{2S_i(2S_i - 1)}} \delta_{vw} f_{au}^{\alpha}$

2.3. Spin-adapted TDA for spin-flip-down excitations (XSF-TDA)

For spin-conserving excitations, X-TD-DFT[27] is a simpler and more accurate alternative than S-TD-DFT obtained simply by a translation rule[26], since it takes into account of spin degeneracy conditions and eliminates double counting of correlation for those already spin-adapted states. Motivated by its success, we extend a similar strategy to spin-flip-down excitations. To this end, we express $A(S_i)$ as

$$\mathbf{A}(S_i) = \mathbf{A}(\infty) + \Delta \mathbf{A}^{\text{TCIS}}(S_i). \tag{21}$$

Since $\mathbf{A}(\infty)$ is just SF-CIS, $\Delta \mathbf{A}^{\text{TCIS}}(S_i)$ can be viewed as a spin adaptation correction, whose matrix elements are provided in Table 3. Note that $\Delta \mathbf{A}^{\text{TCIS}}(S_i) = 0$ for the OO(1) type of excitations, consistent with the spin-complete nature of this excitation class, as previously discussed.

Following the X-TD-DFT framework [27], we define the matrix $\tilde{\mathbf{A}}^{\text{XSF-TDA}}$ in the XSF-TDA eigenvalue equation by

$$\tilde{\mathbf{A}}^{\text{XSF-TDA}} = \mathbf{V}^T [\mathbf{A}^{\text{SF-TDA}} + g_{\mathbf{X}} \Delta \mathbf{A}^{\text{TCIS}}(S_i)] \mathbf{V}, \tag{22}$$

where $\mathbf{A}^{\text{SF-TDA}}$ is given by Eq. (2) for SF-TDA, and $\Delta \mathbf{A}^{\text{TCIS}}(S_i)$ is the spin adaptation correction derived from TCIS, evaluated using orbitals from restricted open-shell Kohan-Sham (ROKS) calculations. In contrast to X-TD-DFT, which mitigates double counting of correlation simply by removing specific excitation couplings[27], we introduce a global hybridization factor $g_{\mathbf{X}}(c_{\mathbf{X}})$, which is a function of the fraction of Hartree-Fock exchange $c_{\mathbf{X}}$. For the Hartree-Fock case $(c_{\mathbf{X}}=1)$, we require $g_{\mathbf{X}}(1)=1$ such that Eq. (22) becomes identical to TCIS. For the case with XC functionals $(c_{\mathbf{X}}<1)$, we require $0 < g_{\mathbf{X}}(c_{\mathbf{X}}) < 1$, such that the double counting of correlation introduced by $\Delta \mathbf{A}^{\text{TCIS}}$ is reduced, meanwhile, non-trivial corrections for spin-contaminated excitations are still present. In this work, we adopted a simple linear function form

$$g_{\rm X}(c_{\rm X}) = (1 - g_{\rm LDA})c_{\rm X} + g_{\rm LDA},$$
 (23)

Table 3. Matrix elements of $\Delta \mathbf{A}^{\text{TCIS}}(S_i)$ for spin-down excitations, where only the upper triangular parts are presented. S_i is the total spin of the ground state, and the matrix elements $f_{pq}^S = \frac{1}{2}(f_{pq}^{\beta} - f_{pq}^{\alpha}) = \frac{1}{2}\sum_t (pt|tq)$.

Block	Matrix elements
CV(1)- $CV(1)$	$\Delta A_{ai,bj} = \frac{1}{S_i} (\delta_{ij} f_{ab}^S + \delta_{ab} f_{ji}^S) \Delta A_{ui,vj} = \frac{2}{2S_i - 1} \delta_{uv} f_{ji}^S - \frac{1}{2S_i - 1} (ui jv)$
CO(1)- $CO(1)$	$\Delta A_{ui,vj} = \frac{1}{2S_{i-1}} \delta_{uv} f_{ji}^{S} - \frac{1}{2S_{i-1}} (ui jv)$
OV(1)- $OV(1)$	$\Delta A_{au,bv} = \frac{1}{2S_{i-1}} \delta_{uv} f_{ab}^{S} - \frac{1}{2S_{i-1}} (au vb)$
CV(1)- $CO(1)$	$\Delta A_{ai,vj} = (\sqrt{\frac{2S_i+1}{2S_i}} - 1)(\delta_{ij} f_{av}^{\beta} - (av ji))$
CV(1)- $OV(1)$	$\Delta A_{ai,bv} = \left(\sqrt{\frac{2S_i + 1}{2S_i}} - 1\right)\left(-\delta_{ab}f_{vi}^{\alpha} - (ab vi)\right)$
CO(1)- $OV(1)$	$\Delta A_{ui,bv} = \frac{1}{2S_i-1}((ui vb) - (ub vi))$
OO(1)- $OO(1)$	$\Delta A_{tu,vw} = 0$
CV(1)- $OO(1)$	$\Delta A_{ai,vw} = -\left(\sqrt{\frac{2S_i + 1}{2S_i - 1}} - 1\right)(av wi) + \frac{1}{S_i}\sqrt{\frac{2S_i + 1}{2S_i - 1}}\delta_{vw}f_{ia}^s$
CO(1)- $OO(1)$	$\Delta A_{ui,vw} = \left(\sqrt{\frac{2S_i}{2S_i - 1}} - 1\right)\left(-\delta_{uv}f_{iw}^{\alpha} - (uv wi)\right) + \frac{1}{\sqrt{2S_i(2S_i - 1)}}\delta_{vw}f_{iu}^{\beta}$
OV(1)-OO(1)	$\Delta A_{au,vw} = \left(\sqrt{\frac{2S_i}{2S_i - 1}} - 1\right) \left(\delta_{wu} f_{av}^{\beta} - (av wu)\right) - \frac{1}{\sqrt{2S_i(2S_i - 1)}} \delta_{vw} f_{au}^{\alpha}$

which contains one empirical parameter g_{LDA} to be fixed. We use $g_{\text{LDA}} = 0.3$ throughout this work, which is fixed by enforcing the desired degeneracy of the $1^1P_{x,y,z}$ states in the calculation for the Be atom (see Sec. 3.2) with the aug-cc-pVTZ basis set. Extending XSF-TDA to more general XC functionals such as range-separated hybrid functionals and exploring more complex function form other than (23) will be explored in future.

2.4. Comparison with related works

In this section, we compare different approaches for addressing spin contamination in SF-CIS and SF-TDA. A summary of the major formal differences among SA-SF-DFT, Q-SF-TDA, MRSF-TDA, and XSF-TDA is provided in Table 4. Below we discuss the key distinctions among these methods are discussed in details.

 $\textbf{Table 4.} \ \ \text{Formal comparison between SA-SF-DFT[5], Q-SF-TDA[29], MRSF-TDA[30], and XSF-TDA.}$

method	reference	spin-adapted configuration	Hermitian	XC functional
SA-SF-DFT[5]	any S_i	all	no	collinear
Q-SF-TDA[29]	any S_i	OO(1)	yes	noncollinear
MRSF-TDA[30]	$S_i = 1$	OO(1), $CO(1)$, $OV(1)$	yes	collinear
XSF-TDA	any S_i	all	yes	noncollinear

SC-SF-CIS[23] include more determinants (for achieving spin completeness) than those necessary for spin-adaptation of SF-CIS. For instance, for the triplet model shown in Fig. 1, SC-SF-CIS includes all the 6 determinants for the CV type into the configuration space, which results in 2 spin-adapted configurations with spin zero. In comparison, TCIS or XSF-TDA employs a minimal set of spin-adapted configurations required to spin-adapt SF-CIS or SF-TDA. To spin-adapt the $CV(\alpha\beta)$ type of

excitation, only the following spin-adapted configuration is included

$$[T_{ai}^{\dagger}(1) \times |S_{i}\rangle\rangle]_{S_{i}-1}^{S_{i}-1}$$

$$= \sqrt{\frac{2S_{i}-1}{2S_{i}+1}} \left(|\Psi_{i}^{\bar{a}}\rangle - \frac{1}{2S_{i}} \sum_{t} (|\Psi_{it}^{a\bar{t}}\rangle - |\Psi_{\bar{i}t}^{\bar{a}\bar{t}}\rangle) - \frac{1}{2S_{i}(2S_{i}-1)} \sum_{tu} |\Psi_{\bar{i}ut}^{a\bar{u}\bar{t}}\rangle \right). \tag{24}$$

Additionally, an important difference between SC-SF-CIS and XSF-TDA is that the latter incorporates dynamical correlation, which is absent in the former.

SA-SF-DFT by Zhang and Herbert[5] employs TEOM of the first kind[22] to derive its equations and uses an empirical matrix element in the form of collinear SF-TD-DFT to translate results from SA-SF-CIS to SA-SF-DFT. Therefore, the dimension of SA-SF-CIS (or SA-SF-DFT) is exactly the same as TCIS (or XSF-TDA). However, a notable difference between TEOM and TCIS in the spin-flip-down case ($S_f = S_i - 1$) is that TEOM yields a non-Hermitian generalized eigenvalue equation due to a nonvanishing coupling in the CV-OO block[5] (as $\langle 0|q_Iq_J^{\dagger} \neq \delta_{IJ}\langle 0|$ in this case), a point that has also been recognized in a recent work by Chibueze and Visscher[29]. Therefore, even SA-SF-CIS itself is actually not a CI-type method. It is not equivalent to neither TCIS introduced in this work nor the SC-SF-CIS approach, a point that has also been realized in Ref. [34].

Q-SF-TDA[29] recently introduced by Chibueze and Visscher[29] can be viewed as an approximation of XSF-TDA, which completely neglects the spin-adaptation correction term in Eq. (22). As a result, only the OO(1) type of excitations is spin-adapted in Q-SF-TDA, and other type of excitations are not corrected. This explains the very similar performance between Q-SF-TDA and USF-TDA observed in Ref. [29].

MRSF-TDA by Lee et al.[30, 31] follows a different strategy, utilizing a mixed-reference reduced density matrix that includes the $M_S = \pm 1$ components of the triplet ground state. Several key differences distinguish MRSF-TDA from XSF-TDA:

- (1) MRSF-TDA is limited to triplet reference, while XSF-TDA is applicable to any high-spin reference.
- (2) MRSF-TDA correctly describes the OO(1), CO(1), and OV(1) types of excitations in the triplet case, but does not correctly describe the spin symmetry of the $CV(\alpha\beta)$ type of excitations[30]. Because it only considers the additional contribution from the last determinant for the $CV(\alpha\beta)$ type in Fig. 1.
- (3) We can recast the MRSF-TDA equation, see Eq. (S8.10) in Supporting Information of Ref. [30], in the form of SF-TDA plus a correction term, which can be written according to the ordering of basis in Eq. (13) (i.e., CV, CO, OV, and OO) as

$$\begin{vmatrix}
-\mathbf{C}_{33} & -\mathbf{C}_{31} & -\mathbf{C}_{32} & \mathbf{0} \\
-\mathbf{C}_{13} & -\mathbf{C}_{11} & -\mathbf{C}_{12} & \mathbf{0} \\
-\mathbf{C}_{23} & -\mathbf{C}_{21} & -\mathbf{C}_{22} & \mathbf{0} \\
\mathbf{0} & \mathbf{0} & \mathbf{0} & \mathbf{0}
\end{vmatrix}, \tag{25}$$

with $(\mathbf{C}_{11})_{ui,wj} = c_{\mathbf{X}} \langle \Psi^{M_S=+1}_{\bar{u}i} | \hat{H} | \Psi^{M_S=-1}_{w\bar{j}} \rangle$ being the introduced coupling between $\Psi^{M_S=+1}_{\bar{u}i}$ and $\Psi^{M_S=-1}_{w\bar{j}}$ originating from the spin-flip transitions from the

 $M_S = +1$ and $M_S = -1$ components of the mixed reference state[30], respectively. Then, it becomes evident that MRSF-TDA lacks corrections for couplings between OO-type excitations and other types. These can be essential for certain cases, see Sec. 3.5.

(4) Another practical difference is that to the best of our knowledge, the current MRSF-TDA implementation in the GAMESS program[35] only supports collinear kernel, whereas we use noncollinear kernel with ALDA0[16] in XSF-TDA, implemented using the PySCF package[36, 37] in this work.

Interestingly, we observe that for the triplet case, although derived from a different approach[30], the final MRSF-TDA corrections for the CO(1) and OV(1) types of excitations are very similar to our correction terms. Specifically, consider the triplet case with two open-shell orbitals u and v shown in Fig. 1, then an example for the MRSF-TDA correction for the CO(1)-CO(1) block reads

$$-(\mathbf{C}_{11})_{ui,uj} = -c_{\mathbf{X}} \langle \Psi_{\bar{u}i}^{M_S=+1} | \hat{H} | \Psi_{u\bar{j}}^{M_S=-1} \rangle$$
$$= -c_{\mathbf{X}} \langle v\bar{j} | | \bar{v}i \rangle = c_{\mathbf{X}} (vi|jv), \tag{26}$$

while in our case, following the second line of Table 3, we have

$$g_{X}\Delta A_{ui,uj} = g_{X}[2f_{ji}^{S} - (ui|ju)]$$

$$= g_{X}[\sum_{t=u,v} (jt|ti) - (ui|ju)] = g_{X}(vi|jv),$$
(27)

which is similar to Eq. (26) except for the prefactor. It should be noted that the parameter $c_{\rm X}$ used in MRSF-TDA (26) and $g_{\rm X}$ defined in Eq. (23) in general take different values. For the BHHLYP functional[38, 39, 40], which is one of the most frequently used XC functionals in MRSF-TDA, $c_{\rm X}=0.5$ and $g_{\rm X}=0.65$ if $g_{\rm LDA}$ is set to 0.3 in the present work.

3. Results

3.1. Benchmark for spin-flip transitions

In this section, we examine how the excited states dominated by the OO-type of excitations are affected by the correction terms introduced in XSF-TDA. We first calculated the quartet excitation energies for 19 open-shell nonlinear molecules with doublet ground states selected from the QUEST database[41] by using spin-flip-down TDA starting from the lowest quartet excited state (denoted by $D\leftarrow Q$) with the aug-cc-pVTZ basis[42]. For comparison, we also performed calculations using spin-flip-up TDA starting from the doublet ground state (denoted by $D\rightarrow Q$), which is free of spin contamination with a ROKS reference[22]. Linear diatomic molecules in the QUEST database are excluded, as either the ground doublet state or the lowest quartet state is spatially degenerate such that the ROKS calculations cannot be applied without breaking the spatial symmetry[43]. Theoretical best estimates (TBEs) of vertical transition energies provided by the QUEST database were used as reference values. We used several XC functionals, including SVWN5[44], BLYP[38, 39], B3LYP[40, 45], BHHLYP[38, 39, 40], and pure Hartree-Fock, which are characterized by increasing proportions of HF exchange.

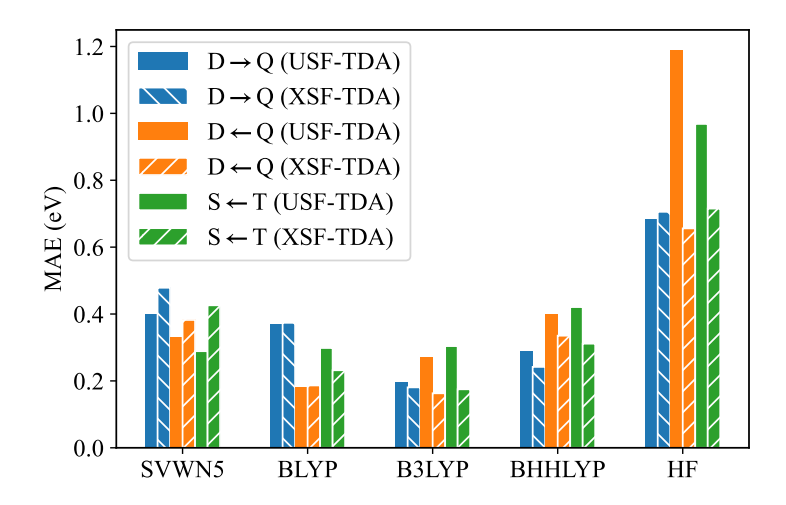


Figure 2. Mean absolute errors (MAEs) in eV of vertical excitation energies computed with spin-flip TDA methods. $D\rightarrow Q$: spin-flip-up SF-TDA with UKS/ROKS reference; $D\leftarrow Q$ and $S\leftarrow T$: spin-flip-down SF-TDA with UKS/ROKS reference. In spin-flip-down XSF-TDA method, Eq. (22) is used, while in spin-flip-up XSF-TDA, the analog of Eq. (1) is used, as there is no spin contamination in such case.

The detailed results obtained using USF-TDA and XSF-TDA methods are summarized in Tables S1 and S2 of the Supporting Information, and the mean absolute errors (MAEs) are displayed in Fig. 2. For USF-TDA, we also compute the change of the expectation value of the square of the total spin angular momentum \hat{S}^2 following Ref. [26], as a diagnostic for spin contaminations. The ideal value for spin-flip-down excitation is $\Delta \langle \hat{S}^2 \rangle = \langle \hat{S}^2 \rangle_{\text{ex}} - \langle \hat{S}^2 \rangle_{\text{gs}} = (S_i - 1)S_i - S_i(S_i + 1) = -2S_i$. As shown in Table S2, the values of $\Delta \langle \hat{S}^2 \rangle$ obtained in USF-TDA only slightly deviate from the ideal value -3 for a quartet reference. Therefore, for these states, USF-TDA can deliver reasonably accurate results. As shown in Fig. 2, XSF-TDA with the same XC functional provides similar performances compared with USF-TDA for these excited states dominated by the OO type of excitations, indicating that introduced spin-adapted correction term does not deteriorate the performance, and hence the double counting of correlation is largely mitigated. To better illustrate this, we performed calculations using XSF-TDA/SVWN5 with other $g_{\rm LDA}$ values. The MAE obtained without spinadapted correction ($g_{LDA} = 0.0$) is 0.36 eV, while that obtained without scaling down the spin-adapted correction ($g_{LDA} = 1.0$) is 0.44 eV. This indicates that the correction term $(g_{LDA} = 1.0)$ introduces double counting that worsens the description of those excited states without spin contamination. Using a smaller value $g_{\rm LDA}=0.3$ gives a MAE of 0.38 eV, which is a reasonably good compromise.

Apart from calculations with a quartet reference, we also computed the excitation energies from the lowest triplet to the singlet ground state (denoted by $S\leftarrow T$) for 89 molecules from the QUEST database using USF-TDA and XSF-TDA with a triplet reference. The detailed results are provided in Table S3. We find that the performances of XSF-TDA for systems with different initial spins are largely consistent, with the difference in MAE being within 0.05 eV. For SVWN5, the MAE of XSF-TDA is slightly larger than that of USF-TDA by 0.14 eV. However, the MAEs of XSF-TDA for BLYP, B3LYP, BHHLYP, and HF are smaller than those of USF-TDA.

3.2. Be and Mg

We next examine the performance of XSF-TDA for excited states involving other types of excitations. We calculated the excitation energies of the 3P_z and $^1P_{x,y,z}$ states for Be and Mg with the 1S ground state, using the USF-TDA and XSF-TDA methods starting from the 3P_z reference state. The involved excitations for 3P_z , 1P_z , $^1P_{x,y}$ are of $O_1O_2(1)$, $O_1O_1(1)$, and OV(1) types. All calculations were performed under the D_{2h} point group symmetry using the 6-31G[46] and aug-cc-pVTZ basis sets. The computed results are summarized in Table 5.

As indicated by the $\Delta \langle \hat{S}^2 \rangle$ values, the 3P_z and 1P_z states are almost free of spin contamination in USF-TDA, for which XSF-TDA give very similar results. In constrast, the $^1P_{x,y}$ states of Be and Mg are severely spin contaminated in USF-TDA. This contamination leads to a substantial reduction in the excitation energy of these states relative to the 1P_z state, while they are expected to be triply degenerate. For example, the splittings between the $^1P_{x,y}$ and 1P_z states computed by USF-TDA with BHHLYP and the aug-cc-pVTZ basis set are 1.2 eV and 0.7 eV for Be and Mg, respectively, while XSF-TDA produces a markedly smaller splittings of only 0.10 eV and 0.25 eV. In general, XSF-TDA consistently produces much smaller energy differences between the 1P_z and $^1P_{x,y}$ states of Be and Mg than USF-TDA with all the tested XC functionals and basis sets. Across all error metrics, including mean error (ME), MAE, standard deviation (SE), and maximum error (MAX), XSF-TDA demonstrates superior performance over USF-TDA.

Table 5. Excited states for Be and Mg obtained using USF-TDA and XSF-TDA with different basis sets. The data in parentheses indicate the values of $\Delta \langle \hat{S}^2 \rangle$ in USF-TDA calculation. The first excited state 3P_z is taken as the reference. ME: mean error, MAE: mean absolute error, SE: standard error, MAX: maximum error.

-	USF-TDA					XSF-TDA						
Basis	AtomState	eExpt.[47	7]SVWN	BLYP	B3LYP	BHHLYP	HF	SVWN	5BLYP	B3LYP	BHHLYF	P HF
6-31G	Be 3P_z	2.73	2.20	2.17	2.33	2.60	2.11	2.20	2.17	2.35	2.59	2.13
			(-2.00)	(-2.00)	(-2.00)	(-2.00)	(-2.00)					
	$^{1}P_{x,t}$	$_{y}$ 5.28	3.88	4.01	3.94	3.79	4.09	4.46	4.61	4.81	5.10	5.97
			,	(-1.00)	(-1.00)	(-1.00)	(-1.00)					
	$^{1}P_{z}$	5.28	4.52	4.82	4.91	5.06	6.04	4.50	4.79	4.87	5.03	5.98
			,	(-1.98)	(-1.99)	(-1.99)	(-1.99)					
	$Mg^{-3}P_z$	2.71	2.66	2.86	2.86	2.94	2.13	2.68	2.87	2.87	2.96	2.17
	1 -		,	(-2.00)	(-2.00)	(-2.00)	(-1.99)					
	$^{1}P_{x,;}$	y = 4.35	3.63	3.88	3.79	3.70	3.46	4.03	4.29	4.38	4.57	4.62
	1		,	(-1.00)	(-1.00)	(-1.00)	(-1.00)					
	$^{1}P_{z}$	4.35	3.96	4.23	4.28	4.43	4.72	3.94	4.18	4.22	4.35	4.54
T TOOL	, D 3D	o =o	,	(-1.95)	(-1.96)	(-1.97)	(-1.93)	2.40				
aug-cc-pVT2	Z Be 3P_z	2.73	2.15	2.25	2.45	2.58	2.06	2.16	2.17	2.35	2.58	2.11
	1 n	- 00	,	(-2.00)	(-2.00)	(-2.00)	(-1.99)	4.10	4.10	4.05	4.00	F 01
	$^{1}P_{x,:}$	y = 5.28	3.64	3.63	3.63	3.58	3.82	4.10	4.12	4.35	4.63	5.21
	$^{1}P_{z}$	F 00	,	(-1.00)	(-1.00)	` /	(-1.00)	4 1 1	4.04	4.20	4.59	F 00
	$^{-}P_{z}$	5.28	4.17	4.37	4.55	4.78	5.61	4.11	4.24	4.39	4.53	5.20
	$Mg^{-3}P_z$	2.71	(-1.93) 2.67	(-1.93) 2.91	(-1.92)	(-1.93) 2.92	(-1.83) 2.06	2.69	2.92	2.80	2.96	0.14
	$Mg^{-3}P_z$	2.11		(-2.00)	2.87 (-2.00)	(-2.00)	(-1.99)	2.09	2.92	2.89	2.90	2.14
	$^{1}P_{x,j}$	4.35	(-2.00) 3.59	3.82	(-2.00) 3.73	(-2.00) 3.64	3.30	3.93	4.15	4.23	4.38	4.19
	x	y 4.30		(-1.00)	(-1.00)	(-1.00)	(-1.00)	5.35	4.10	4.20	4.50	4.13
	$^{1}P_{z}$	4.35	3.87	4.12	4.19	4.34	4.50	3.83	4.01	4.05	4.14	4.12
	1 z	4.55		(-1.89)	(-1.91)	(-1.91)	(-1.74)	3.03	4.01	4.00	4.14	4.12
	ME		-0.71	-0.53	-0.49	-0.42	-0.46	-0.56	-0.41	-0.30	-0.13	-0.09
	MAE		0.71	0.59	0.54	0.51	0.73	0.56	0.47	0.36	0.26	0.39
	SE		0.47	0.52	0.53	0.60	0.67	0.36	0.41	0.34	0.31	0.45
	MAX		-1.64	-1.65	-1.65	-1.70	-1.46	1.18	1.16	0.93	0.75	0.70

3.3. Potential energy curves for HF

Apart from the excitation energies due to spin-flip transitions, we also applied XSF-TDA for computing the potential energy curve (PEC) of HF, which is a typical testbed for spin-flip methods[23, 1]. We take the same reference state $^3\Sigma$ with the electronic configuration $1\sigma^22\sigma^21\pi^43\sigma^14\sigma^1$ as in previous works[23] to compute the PEC of the ground state using SF-TDA. The PECs obtained using USF-TDA and XSF-TDA with the aug-cc-pVTZ basis set are shown in Fig. 3(a). For comparison, we also show the PECs obtained with MRSF-TDA[30] in Fig. 3(b). To make a fair comparison, we make sure that the same reference state is obtained, by passing the converged results from PySCF as initial guess to GAMESS through MOKIT[48] and using the maximum overlap method (MOM)[49] in ROKS calculations. In Figs. 3(a) and 3(b), the PEC obtained from NEVPT4(SD) (fully internally contracted partial fourth-order N-electron valence perturbation theory)[50] with a CAS(8e,50) active space using the ORCA package [51, 52] is shown as a reference.

As shown in Fig. 3(a), the PECs obtained by XSF-TDA agree well with those obtained by USF-TDA for SVWN5, BLYP and B3LYP, while the results differ for BHHLYP and pure HF at large bond distances. To better understand such behaviors, we plot $\Delta \langle \hat{S}^2 \rangle$ obtained in USF-TDA in Fig. 3(c). It is clear that at large bond distance, the results obtained with BHHLYP and pure HF show a significant amount of spin contamination, which in turn leads to the growing discrepancies between the XSF-TDA and USF-TDA results observed in Fig. 3(a). The increase of $\Delta \langle \hat{S}^2 \rangle$ can be explained by the increase of $CO(\alpha\beta)$ type of excitations as demonstrated in Fig. 3(d). At shorter bond lengths, the ground state is primarily reached by $OO(\alpha\beta)$ -type excitations. As the bond length increases, the dominant configuration gradually changes to a $CO(\alpha\beta)$ -type excitation.

In comparison, we find that the MRSF-TDA result with pure HF is very close to the USF-TDA result, see Fig. 3(b), likely due to the missing of the coupling between the OO and other types of excitations in the correction (25). The major difference between the PECs of MRSF-TDA and those of USF-TDA with other XC functionals can be attributed to the use of collinear functionals in the former case. In particular, for SVWN5 and BLYP, the correction term in MRSF-TDA reduce to zero, causing the results to coincide with those of collinear SF-TDA, while the USF-TDA results are obtained with the noncollinear kernel (5).

3.4. Potential energy curves for F_{g}

The F₂ molecule is a challenging system for electronic structure methods due to the coexistence of strong dynamical and nondynamical correlation effects. We investigated its PEC using SF-TDA methods with the aug-cc-pVTZ basis set. from the high-spin $^3\Sigma_u^+$ reference state with the electronic configuration $1\sigma_g^21\sigma_u^22\sigma_g^22\sigma_u^23\sigma_g^11\pi_u^41\pi_g^43\sigma_u^1$. The resulting PECs obtained from USF-TDA, XSF-TDA, and MRSF-TDA are shown in Figs. 4(a) and 4(b), along with the NEVPT4(SD) results using a CAS(14e,8o) active space. For this system, we find that the PECs obtained by USF-TDA and XSF-TDA are qualitatively similar for all the considered XC functionals. This is explained by the negligible amount of spin contamination in the USF-TDA results shown in Fig. 4(c). For pure HF, the MRSF-TDA result using a ROKS reference almost coincides with the USF-TDA result, which is also observed in the calculations of the HF molecule. However, the PECs of MRSF-TDA with other XC functionals tend to be higher than the corresponding USF-TDA results at larger bond distance, which is likely attributed

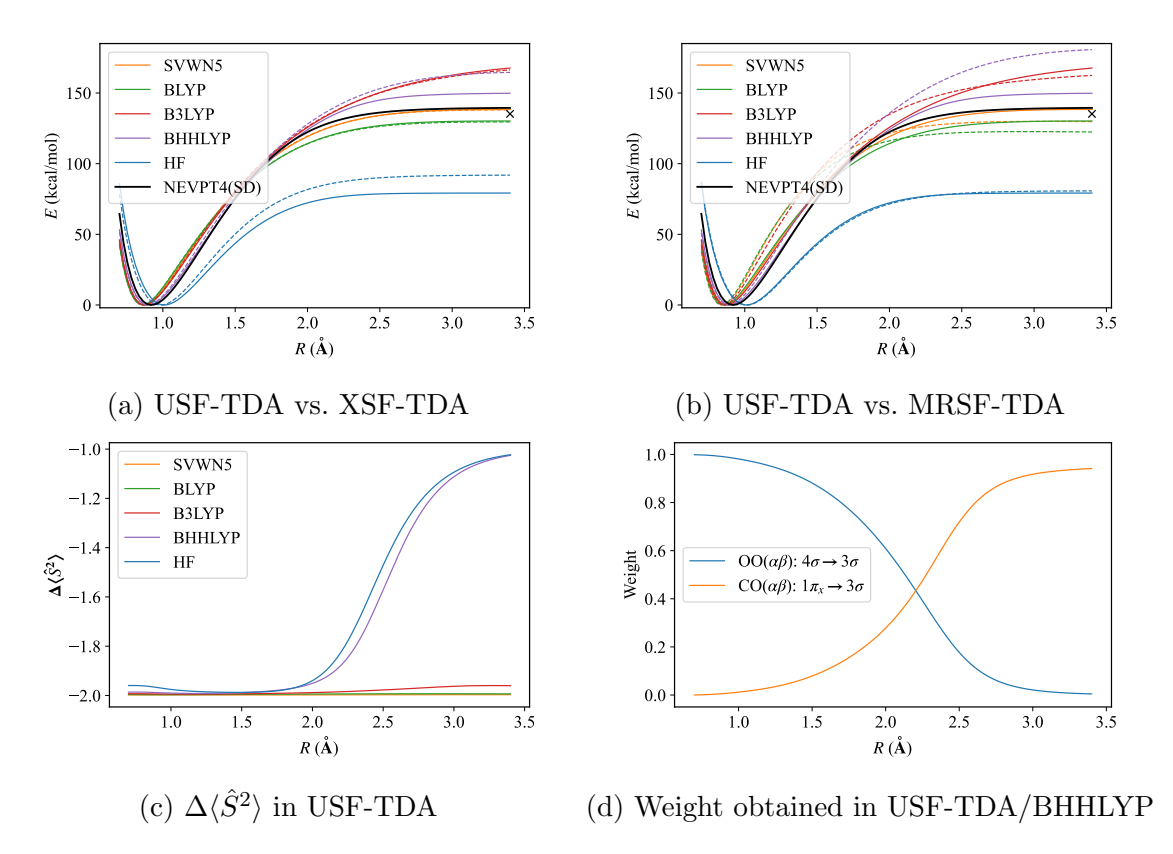


Figure 3. Results for the HF molecule using SF-TDA methods with the aug-cc-pVTZ basis set. (a) PECs obtained with USF-TDA (solid) and XSF-TDA (dashed); (b) PECs obtained with USF-TDA (solid) and MRSF-TDA (dashed); (c) $\Delta \langle \hat{S}^2 \rangle$ obtained in USF-TDA; (d) Weights of the dominant two excitations obtained in USF-TDA/BHHLYP. The minimum of each curve in (a) and (b) has been shifted to zero for a better comparison. The cross marker in (a) and (b) represents the experimental bond dissociation energy 135.1 kcal/mol[53].

to the use of collinear functionals.

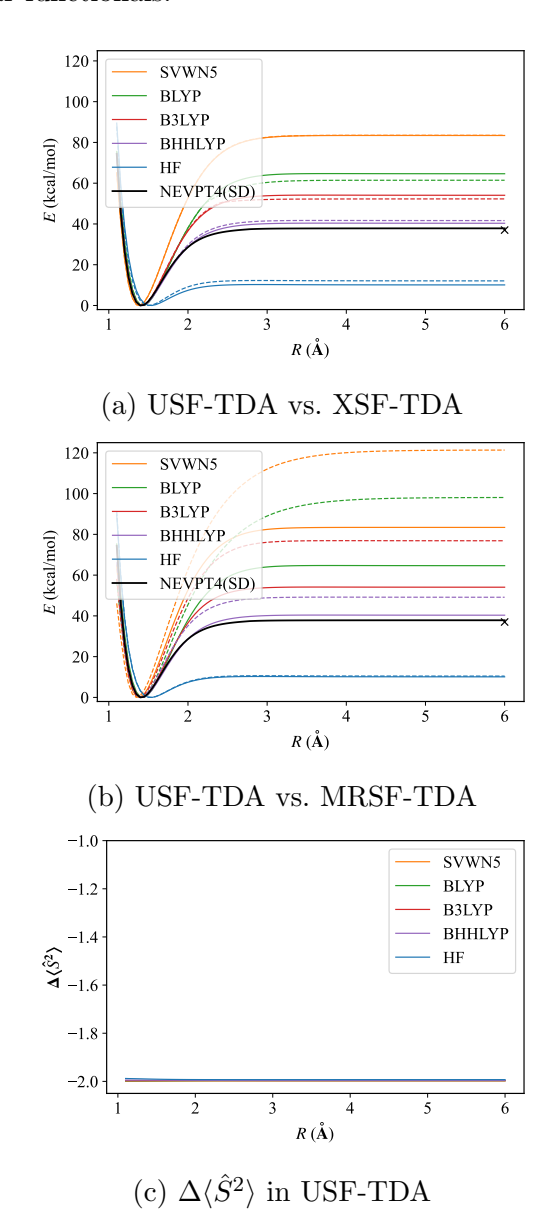


Figure 4. Results for the F_2 molecule using SF-TDA methods with the aug-cc-pVTZ basis set. (a) PECs obtained with USF-TDA (solid) and XSF-TDA (dashed); (b) PECs obtained with USF-TDA (solid) and MRSF-TDA (dashed); (c) $\Delta \langle \hat{S}^2 \rangle$ in USF-TDA. The minimum of each curve in (a) and (b) has been shifted to zero for a better comparison. The cross marker in (a) and (b) represents the experimental bond dissociation energy 37.0 kcal/mol[54].

3.5. Inverted singlet-triplet gap systems

The inverted singlet-triplet gap (abbreviated as INVEST) systems, in which the Hund's rule is violated for the lowest singlet (S_1) and triplet (T_1) excited states, have recently gained a lot of interests [55, 56, 57, 58, 59, 60, 61, 62, 63, 64, 65, 66, 67, 68, 69] due to their potential in optelectronic applications such as organic light-emitting diodes (OLED). Unfortunately, standard spin-conserving TD-DFT cannot correctly

describe the correct ordering of S_1 and $T_1[56]$, except for some doubly hybrid functionals [60]. Here, we apply spin-conserving and spin-flip TDA methods to the benchmark set by Loos et al. [70], see Fig. 5(a), which contains 10 molecules with negative $\Delta E_{\rm ST} = E(S_1) - E(T_1) < 0$. The molecular coordinates were optimized at the level of CCSD(T)/cc-pVTZ (within the frozen-core approximation), and TBEs for $\Delta E_{\rm ST}$ were obtained from CC3/aug-cc-pVTZ + [CCSDT/6-31+G(d) - CC3/6-31+G(d)] for S_1 and CC3/aug-cc-pVDZ + [CCSD/aug-cc-pVTZ - CCSD/aug-cc-pVDZ] for T_1 , respectively. For spin-conserving TDA, $\Delta E_{\rm ST}$ is obtained from two separate TDA calculations for S_1 and T_1 , respectively, starting from the closed-shell ground state S_0 , while for spin-flip-down TDA, $\Delta E_{\rm ST}$ is taken as the excitation energy of the second singlet excited state ω_1 with respect to the triplet reference T_1 . [Note that the excitation energy of the first singlet excited state ω_0 is the energy difference between S_0 and T_1 . Fig. 5(b) displays the obtained $\Delta E_{\rm ST}$ by spin-conserving TDA, USF-TDA, MRSF-TDA, XSF-TDA with the 6-31G* and aug-cc-pVTZ basis sets using the following XC functionals: SVWN5[44], BLYP[39, 38], PBE[71], B3LYP[40, 45], PBE0[72, 73], and BHHLYP[38, 39, 40]. For both MRSF-TDA and XSF-TDA, the ROKS reference is used and the stability of the solution has been checked. For the molecules 9 and 10, some solutions obtained with pure density functionals were found unstable, and in such case we used the occupation obtained with in BHHLYP calculations to obtain a stable solution. Detailed results are summarized in Table S4-S7.

As shown in Fig. 5(b), the obtained $\Delta E_{\rm ST}$ in both spin-conserving and spin-flipdown TDA show a weak dependence on the basis set. Conventional spin-conserving TDA gives all positive $\Delta E_{\rm ST}$, agree with previous studies [56, 60]. USF-TDA with BHHLYP can give negative $\Delta E_{\rm ST}$ for a few systems, while other XC functionals can only give negative values for the last two systems. Notably, while the excited state S_1 is dominated by the $OO(\alpha\beta)$ type of excitations, we find that results of USF-TDA with hybrid functionals display substantial amount of spin contamination (see Tables S4 and S6). For MRSF-TDA, most of $\Delta E_{\rm ST}$ are also positive. Special double tuning of the parameters in XC functionals is required to achieve good performance, as demonstrated in a recent study [69]. [NB: the energy of T_1 in Ref. [69] is taken as the energy obtained in a second MRSF-TDA calculation for the lowest triplet. In Table S8, we made a comparison of results obtained by these two approaches.] Quite remarkably, XSF-TDA with B3LYP and PBE0 show very good performances, with MAEs being 0.07 eV and 0.10 eV, respectively, for results using the aug-cc-pVTZ basis set (see Table S7). We attribute the better performance of XSF-TDA over other spin-flip TDA methods to the presence of the coupling between the OO(1) and other type of excitations in the spin-adapted corrections, see the last three lines in Table 3. In contrast, such couplings are missing in MRSF-TDA, see Eq. (25). In particular, the coupling between the OO(1) and CV(1) type of excitations can increase the percentage of CV(1) type of excitations in the S_1 state, which is responsible for the dynamical spin polarization [74, 68, 69] that is essential for obtaining negative $\Delta E_{\rm ST}$. Besides, the too negative $\Delta E_{\rm ST}$ obtained from XSF-TDA/BHHLYP suggest that it is worthwhile to systematically explore the choice of g_X in future work.

4. Conclusion

In this work, we introduced a simple and accurate method for resolving the spin contamination problem in SF-TDA, extending on our previous work for spin-conserving excitations[22, 26, 27]. Benchmark calculations demonstrate that the proposed XSF-

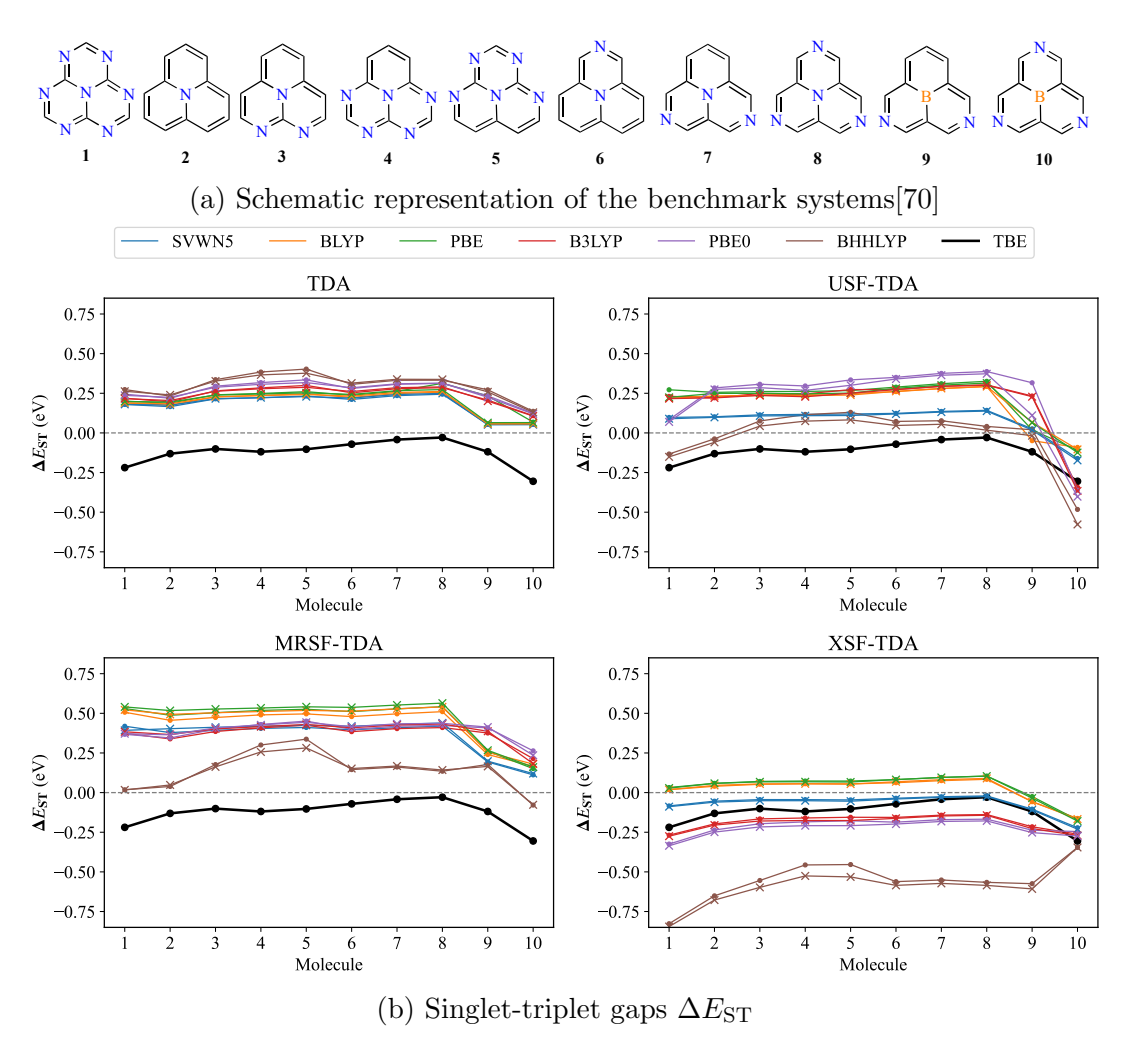


Figure 5. Results for inverted single-triplet gap systems. (a) Schematic representation of heptazine (no. 1) and cyclazine (no. 2) and their derivatives considered in Ref. [70] as benchmark systems. (b) Singlet-triplet gaps $\Delta E_{\rm ST}$ (in eV) computed using TDA and SF-TDA methods with the 6-31G* (cross) and aug-cc-pVTZ (dot) basis sets. The theoretical best estimates (TBEs) are taken from Ref. [70].

TDA offers comparable accuracy as USF-TDA for excited states without significant amount of spin contamination, but dramatically improves upon USF-TDA for heavily spin contaminated excited states. We have also made both formal and numerical between XSF-TDA and MRSF-TDA[30], demonstrating the superiority of XSF-TDA in dealing with complex electronic structure problems such as the inverted singlet-triplet gap systems[60].

This work opens up many promising directions to be explored in future: (1) While XSF-TDA with the simple parameterization in Eq. (23) adopted in this work has been demonstrated to be superior to USF-TDA, there is still room for improving its performance by systematic optimization of g_X against a broader benchmark. (2) The combination of multicollinear functionals[18, 19, 20] with XSF-TDA is straightforward and further comparison with ALDA0[16] will be made. (3) Implementing spin-orbit couplings among different spin states[75, 76, 77] and nonadiabatic couplings between excited states[78, 79, 80] will enable the study of nonadiabatic excited-state dynamics for open-shell systems. Progress along these lines will be reported in due time.

Acknowledgment

This work is dedicated to Prof. Wenjian Liu on the occasion of his 60th birthday. The authors acknowledge Zikuan Wang, Jingxiang Zou, Bohan Zhang for critically reading the manuscript. This work was supported by the Quantum Science and Technology-National Science and Technology Major Project(2023ZD0300200) and the Fundamental Research Funds for the Central Universities.

References

- Y. Shao, M. Head-Gordon and A.I. Krylov, J. Chem. Phys. 118 (11), 4807–4818 (2003).
- [2] D. Casanova and A.I. Krylov, Phys. Chem. Chem. Phys. **22** (8), 4326–4342 (2020).
- [3] W.R. Kitzmann, J. Moll and K. Heinze, Photochem. Photobiol. Sci. 21 (7), 1309–1331 (2022).
- [4] W.R. Kitzmann and K. Heinze, Angew. Chem. Int. Ed 62 (15), e202213207 (2023).
- [5] X. Zhang and J.M. Herbert, J. Chem. Phys. **143** (23), 234107 (2015).
- [6] J. Mato and M.S. Gordon, J. Phys. Chem. A 123 (6), 1260–1272 (2019).
- [7] Y. Harabuchi, K. Keipert, F. Zahariev, T. Taketsugu and M.S. Gordon, J. Phys. Chem. A 118 (51), 11987–11998 (2014).
- [8] J.M. Herbert and A. Mandal, in *Time-dependent density functional theory* (Jenny Stanford Publishing, Singapore, 2022), pp. 361–404.
- [9] F. Wang and T. Ziegler, J. Chem. Phys. **121** (24), 12191–12196 (2004).
- [10] F. Wang and T. Ziegler, J. Chem. Phys. **122** (7), 074109 (2005).
- [11] F. Wang and W. Liu, J. Chin. Chem. Soc. **50** (3B), 597–606 (2003).
- [12] J. Gao, W. Liu, B. Song and C. Liu, J. Chem. Phys. 121 (14), 6658–6666 (2004).
- [13] J. Gao, W. Zou, W. Liu, Y. Xiao, D. Peng, B. Song and C. Liu, J. Chem. Phys. 123 (5), 054102 (2005).
- [14] Z. Rinkevicius, O. Vahtras and H. Ågren, J. Chem. Phys. 133 (11), 114104 (2010).
- [15] Y.A. Bernard, Y. Shao and A.I. Krylov, J. Chem. Phys. 136 (20), 204103 (2012).
- [16] Z. Li and W. Liu, J. Chem. Phys. **136** (2), 024107 (2012).

- [17] Z. Li and W. Liu, J. Chem. Theor. Comput. 12 (6), 2517–2527 (2016).
- [18] H. Li, Z. Pu, Q. Sun, Y.Q. Gao and Y. Xiao, J. Chem. Theor. Comput. 19 (8), 2270–2281 (2023).
- [19] X. Zhang and Y. Xiao, arXiv preprint arXiv:2505.17766 (2025).
- [20] T. Wang, H. Li, Y.Q. Gao and Y. Xiao, J. Chem. Theor. Comput. 21 (14), 6905–6921 (2025).
- [21] M.E. Casida, J. Chem. Phys. **122** (5), 054111 (2005).
- [22] Z. Li and W. Liu, J. Chem. Phys. **133** (6), 157 (2010).
- [23] J.S. Sears, C.D. Sherrill and A.I. Krylov, J. Chem. Phys. 118 (20), 9084–9094 (2003).
- [24] O. Vahtras and Z. Rinkevicius, J. Chem. Phys. **126** (11), 114101 (2007).
- [25] D. Rowe and C. Ngo-Trong, Rev. Mod. Phys. 47 (2), 471 (1975).
- [26] Z. Li, W. Liu, Y. Zhang and B. Suo, J. Chem. Phys. 134 (13), 134101 (2011).
- [27] Z. Li and W. Liu, J. Chem. Phys **135** (19), 194106 (2011).
- [28] Z. Li and W. Liu, J. Chem. Theor. Comput. 12 (1), 238–260 (2016).
- [29] C.S. Chibueze and L. Visscher, J. Chem. Phys. **163** (9), 094111 (2025).
- [30] S. Lee, M. Filatov, S. Lee and C.H. Choi, J. Chem. Phys. 149 (10), 104101 (2018).
- [31] S. Lee, E.E. Kim, H. Nakata, S. Lee and C.H. Choi, J. Chem. Phys. 150 (18), 184111 (2019).
- [32] P. Jørgensen, Second quantization-based methods in quantum chemistry (Elsevier, Amsterdam, Netherlands, 2012).
- [33] R. Pauncz, Spin Eigenfunctions (Springer US, New York, 1979).
- [34] Z. Wang, Z. Li, Y. Zhang and W. Liu, J. Chem. Phys. **153** (16) (2020).
- [35] G.M.J. Barca, C. Bertoni, L. Carrington, D. Datta, N. De Silva, J.E. Deustua, D.G. Fedorov, J.R. Gour, A.O. Gunina, E. Guidez, T. Harville, S. Irle, J. Ivanic, K. Kowalski, S.S. Leang, H. Li, W. Li, J.J. Lutz, I. Magoulas, J. Mato, V. Mironov, H. Nakata, B.Q. Pham, P. Piecuch, D. Poole, S.R. Pruitt, A.P. Rendell, L.B. Roskop, K. Ruedenberg, T. Sattasathuchana, M.W. Schmidt, J. Shen, L. Slipchenko, M. Sosonkina, V. Sundriyal, A. Tiwari, J.L. Galvez Vallejo, B. Westheimer, M. Wloch, P. Xu, F. Zahariev and M.S. Gordon, J. Chem. Phys. 152 (15), 154102 (2020).
- [36] Q. Sun, X. Zhang, S. Banerjee, P. Bao, M. Barbry, N.S. Blunt, N.A. Bogdanov, G.H. Booth, J. Chen, Z.H. Cui et al., J. Chem. phys. 153 (2), 024109 (2020).
- [37] Q. Sun, T.C. Berkelbach, N. Blunt, G.H. Booth, S. Guo, Z. Li, J. Liu, J.D. Mcclain, E. Sayfutyarova and S. Sharma, Wires. Comput. Mol. Sci 8 (1), e1340 (2018).
- [38] A.D.P. Becke, Phys. Rev. A **38** (6), 3098–3100 (1988).
- [39] C. Lee, W. Yang and R.G. Parr, Phys. Rev. B **37** (2), 785–789 (1988).
- [40] A.D. Becke, J. Chem. Phys. **98** (7), 5648–5652 (1993).
- [41] P.F. Loos, M. Boggio-Pasqua, A. Blondel, F. Lipparini and D. Jacquemin, J. Chem. Theor. Comput. 21 (16), 8010–8033 (2025).
- [42] T.H. Dunning, J. Chem. Phys. **90**, 1007–1023 (1989).
- [43] M. Seth and T. Ziegler, J. Chem. Phys. **123** (14), 144105 (2005).
- [44] S.H. Vosko, L. Wilk and M. Nusair, Can. J. Phys. 58 (8), 1200–1211 (1980).
- [45] P.J. Stephens, F.J. Devlin, C.F. Chabalowski and M.J. Frisch, J. Phys. Chem. 98 (1-3), 247–257 (1994).
- [46] R. Krishnan, J.S. Binkley, R. Seeger and J.A. Pople, J. Chem. Phys. 72 (1), 650–654 (1980).
- [47] A. Kramida, Y. Ralchenko, J. Reader and N.A. Team, NIST Atomic Spectra Database (version 5.1) [online] 2013.

- [48] J. Zou, Molecular Orbital Kit (MOKIT), https://gitlab.com/jxzou/mokit 2025, (accessed Jun 25, 2025).
- [49] A.T.B. Gilbert, N.A. Besley and P.M.W. Gill, J. Phys. Chem. A 112 (50), 13164–71 (2008).
- [50] E.M. Kempfer, K. Sivalingam and F. Neese, J. Chem. Theor. Comput. 21 (8), 3953–3967 (2025).
- [51] F. Neese, F. Wennmohs, U. Becker and C. Riplinger, J. Chem. Phys. 152 (22), 224108 (2020).
- [52] F. Neese, WIRES Comput. Molec. Sci. 12 (5), e1606 (2022).
- [53] B. De Darwent, NSRDS-NBS 31 (1970).
- [54] P. Wang, S. Gong and Y. Mo, J. Phys. Chem. Lett. 15 (51), 12594–12600 (2024).
- [55] J. Ehrmaier, E.J. Rabe, S.R. Pristash, K.L. Corp and W. Domcke, J. Phys. Chem. A 123 (38), 8099–8108 (2019).
- [56] P. de Silva, J. Phys. Chem. Lett. 10 (18), 5674–5679 (2019).
- [57] G. Ricci, E. San-Fabián, Y. Olivier and J.C. Sancho-García, Chem. Phys. Chem. 22 (6), 553–560 (2021).
- [58] R. Pollice, P. Friederich, C. Lavigne, G.D.P. Gomes and A. Aspuru-Guzik, Matter 4 (5), 1654–1682 (2021).
- [59] F. Dinkelbach, M. Bracker, M. Kleinschmidt and C.M. Marian, J. Phys. Chem. A 125 (46), 10044–10051 (2021).
- [60] S. Ghosh and K. Bhattacharyya, J. Phys. Chem. A 126 (8), 1378–1385 (2022).
- [61] N. Aizawa, Y.J. Pu, Y. Harabuchi, A. Nihonyanagi, R. Ibuka, H. Inuzuka, B. Dhara, Y. Koyama, K.i. Nakayama, S. Maeda et al., Nature 609 (7927), 502–506 (2022).
- [62] G. Ricci, J.C. Sancho-García and Y. Olivier, J. Mater. Chem. C 10, 12680–12698 (2022).
- [63] L. Tučková, M. Straka, R.R. Valiev and D. Sundholm, Phys. Chem. Chem. Phys. 24, 18713–18721 (2022).
- [64] E. Monino and P.F. Loos, J. Chem. Phys. **159** (3), 034105 (2023).
- [65] D. Drwal, M. Matousek, P. Golub, A. Tucholska, M. Hapka, J. Brabec, L. Veis and K. Pernal, J. Chem. Theor. Comput. 19 (21), 7606–7616 (2023).
- [66] J.T. Blaskovits, M.H. Garner and C. Corminboeuf, Angew. Chem. Int. Ed 62, e202218156 (2023).
- [67] A. Dreuw and M. Hoffmann, Front. Chem. 11, 1239604 (2023).
- [68] D. Drwal, M. Matousek, P. Golub, A. Tucholska, M. Hapka, J. Brabec, L. Veis and K. Pernal, J. Chem. Theory Comput. 19 (21), 7606–7616 (2023).
- [69] A. Lashkaripour, W. Park, M. Mazaherifar and C.H. Choi, J. Chem. Theory Comput. 21 (11), 5661–5668 (2025).
- [70] P.F. Loos, F. Lipparini and D. Jacquemin, J. Phys. Chem. Lett. 14 (49), 11069–11075 (2023).
- [71] J.P. Perdew, K. Burke and M. Ernzerhof, Phys. Rev. Lett. 77 (18), 3865–3868 (1998).
- [72] M. Ernzerhof and G.E. Scuseria, J. Chem. Phys. 110 (11), 5029–5036 (1999).
- [73] C. Adamo and V. Barone, J. Chem. Phys. 110 (13), 6158–6170 (1999).
- [74] H. Kollmar and V. Staemmler, Theor. Chim. Acta 48 (3), 223–239 (1978).
- [75] F. Wang and T. Ziegler, J. Chem. Phys. **123** (15), 154102 (2005).
- [76] Z. Li, B. Suo, Y. Zhang, Y. Xiao and W. Liu, Mol. Phys. 111 (24), 3741–3755 (2013).
- [77] C.S. Chibueze and L. Visscher, J. Chem. Phys. **161** (9), 094112 (2024).
- [78] Z. Li and W. Liu, J. Chem. Phys. **141** (1), 014110 (2014).

- [79] Z. Li, B. Suo and W. Liu, J. Chem. Phys. ${\bf 141}$ (24), 244105 (2014). [80] X. Zhang and J.M. Herbert, J. Chem. Phys. ${\bf 141}$ (6), 064104 (2014).